Available online at www.sciencedirect.com
ScienceDirect
International Journal of Thermal Sciences 48 (2009) 602–617
International Journal of Thermal Sciences
www.elsevier.com/locate/ijts

Influence of the shape of the nozzle on local heat transfer distribution between smooth flat surface and impinging air jet

Puneet Gulati, Vadiraj Katti, S.V. Prabhu *

Department of Mechanical Engineering, I.I.T., Bombay, Mumbai, India

Received 26 October 2007; received in revised form 17 December 2007; accepted 5 May 2008

Available online 16 June 2008

Abstract

An experimental investigation is performed to study the effects of the shape of the nozzle, jet-to-plate spacing and Reynolds number on the local heat transfer distribution to normally impinging submerged air jet on smooth and flat surface. Three different nozzle cross-sections, *viz.* circular, square, and rectangular, each with an equivalent diameter of around 20 mm are used during this study. Reynolds number based on hydraulic diameter (d) is varied between 5000 and 15000 and jet-to-plate spacing from 0.5 to 12 nozzle diameters. Length-to-equivalent diameter ratio (l/de) of 50 is chosen for each nozzle configuration. The local heat transfer characteristics are estimated using thermal images obtained by infrared thermal imaging technique. Local and average Nusselt number on the impinged surface are presented for all the nozzle configurations investigated. Pressure drop measurements across nozzles are made and pressure loss coefficient for all nozzle configurations is reported. Average Nusselt numbers are found to be insensitive to the shape of the nozzle.

Keywords: Impinging jet; Shape of the nozzle; Local heat transfer; Pressure drop; Thermal imaging

1. Introduction

Impinging jets have received considerable attention due to their inherent characteristics of high rates of heat transfer besides having simple geometry. Such impinging flow devices allow for short flow paths and relatively high rates of cooling from comparatively small surface area. Various industrial processes involving high heat transfer rates apply impinging jets. Few industrial processes which employ impinging jets are drying of food products, textiles, films and papers; processing of some metals and glass, cooling of gas turbine blades and outer wall of the combustion chamber, cooling of electronic equipments, etc. Heat transfer rates in case of impinging jets are affected by various parameters like Reynolds number, jet-to-plate spacing, radial distance from stagnation point, Prandtl number, target plate inclination, confinement of the jet, nozzle geometry, curvature of target plate, roughness of the target plate and turbulence intensity at the nozzle exit.

Many prior studies are mostly on jet impinging over flat and smooth surface. Review of the experimental work on heat transfer to impinging jets is reported by Livingood and Hrycak [1], Martin [2], Jambunathan et al. [3] and Viskanta [4]. Gardon and Cobonpue [5] reported the heat transfer distribution between circular jet and flat plate for the nozzle plate spacing greater than two times the diameter of jet, both for single jet and array of jets. Specially designed heat flux gage were used for the measurement of local heat transfer distribution from a constant wall temperature plate. Gardon and Akfirat [6] studied the effect of turbulence on the heat transfer between two dimensional jet and flat plate. Gardon and Akfirat [7] studied effect of multiple two-dimensional jets on the heat transfer distribution. Baughn and Shimizu [8] and Hrycak [9] conducted experiments of heat transfer to round jet from flat plate employing different methods of surface temperature measurement. Lytle and Webb [10] studied the effect of very low nozzle-to-plate spacing ($z/d < 1$) on the local heat transfer distribution on a flat plate impinged by a circular air jet issued by long pipe nozzle which allows for fully developed flow at the nozzle exit and found that in the acceler-

* Corresponding author. Tel.: +91 22 25767515; fax: +91 22 25726875, 25723480.

E-mail addresses: svprabhu@me.iitb.ac.in, svprabhu@iitb.ac.in (S.V. Prabhu).

1290-0729/$ – see front matter
doi:10.1016/j.ijthermalsci.2008.05.002

Nomenclature

A	surface area for smooth surface	m^2	
d	hydraulic diameter	m	
de	equivalent diameter	m	
DP	pressure drop across the nozzle	Pa	
h	heat transfer coefficient	$W/m^2\,K$	
h_o	heat transfer coefficient at the stagnation point	$W/m^2\,K$	
I	current	A	
k	thermal conductivity of air	W/m K	
K	pressure loss coefficient ($DP/0.5\rho\bar{V}^2$)		
l	length of the nozzle pipe	m	
Nu	Nusselt number (hd/k)		
Nu_o	stagnation Nusselt number ($h_o d/k$)		
q	heat flux	W/m^2	
q_{conv}	net heat flux convected to the impinging jet	W/m^2	
q_{joule}	imposed Ohmic heat flux, (VI/A)	W/m^2	
q_{loss}	total heat flux loss from impingement plate	W/m^2	
$q_{rad(f)}$	radiation heat loss from the front surface of impingement plate	W/m^2	
$q_{rad(b)}$	radiation heat loss from the back surface of impingement plate	W/m^2	
q_{nat}	heat loss by natural convection from the back surface of impingement plate	W/m^2	
r	radial distance from the stagnation point	m	
Re	Reynolds number ($\rho\bar{V}d/\mu$)		
T_j	jet air temperature	°C	
T_r	temperature of the target plate at given radial location	°C	
$\bar{V}$	average velocity at the exit of the nozzle	m/s	
V	voltage	V	
z	nozzle plate spacing	m	
AR	aspect ratio		
Greek symbols:			
μ	viscosity of air	Pa s	
ν	kinematic viscosity of jet fluid	m^2/s	
ρ	density of air corresponding to supply pressure	kg/m^3	

ation range of the nozzle plate spacing ($z/d < 0.25$), maximum Nusselt number shifts from the stagnation point to the point of secondary peak with the effect being more pronounced at higher Reynolds number. Lee et al. [11] studied the effect of nozzle diameter on impinging jet heat transfer and fluid flow. They reported that local Nusselt numbers in the region corresponding to $0 \leqslant r/d \leqslant 0.5$ are increased with increasing nozzle diameter. Beitelmal et al. [12] analyzed two-dimensional impinging jets and correlated heat transfers in the stagnation point, stagnation region and wall jet region with approximate solutions developed using simplified flow assumptions. Theoretical solutions in the wall jet region fit better at large distances from stagnation point. Lienhard [13] analyzed heat transfer by impingement of circular free-surface liquid jets and analytical solutions were explained for heat transfer in different regions on the target plate. Hofmann et al. [14] performed an experimental investigation on flow structure and heat transfer from a single round jet impinging perpendicularly on a flat plate. They proposed a correlation for local Nusselt number in impinging axisymmetric jets as $Nu = 0.55[Re^3 + 10Re^2]^{0.25} \cdot Pr^{0.42} \cdot e^{-0.025(r/d)^2}$, for $14000 < Re < 230000$, $0.5 < z/d < 10$, and $0 < r/d < 8$. O'Donovan and Murray [15] investigated the turbulent fluctuations within the wall jet to study the fluid flow and convective heat transfer mechanisms that influence the magnitude and location of secondary peaks. They reported that at low nozzle to impingement surface spacings the mean heat transfer distribution in the radial direction exhibits secondary peaks. O'Donovan and Murray [16] studied the influence of the actual vortex flow structure, at various stages of its development, on the convective heat transfer in the wall jet region.

There have been a few studies which investigated the effects of nozzle configuration on the impinging jet heat transfer. Pan et al. [17] and Stevens et al. [18] studied the effect of nozzle configuration on impingement heat transfer and fluid flow characteristics for unconfined free surface water jet. It was shown that about 40% enhancements in heat transfer were possible with sharp edged orifice when compared with long pipe. This was attributed to higher turbulence intensities at the exit of sharp edged orifice. Garimella and Nenaydykh [19] conducted series of experiments to study the effect of nozzle length to diameter ratio on impingement heat transfer rates to confined submerged liquid jet of FC-77. They reported that square edged orifice of l/d less than 0.5 provide better heat transfer characteristics when compared with larger l/d. Lee and Lee [20] studied the effect of nozzle configuration for l/d of 0.2 with three different types of profiles at nozzle exit i.e. square edged, standard-edged and sharp edged orifices. The tests were carried out for unconfined air jets impinging normally on smooth flat surface and the heat transfer results show that at stagnation region sharp edged orifice performs better. Brignoni and Garimella [21] studied the effect of nozzle inlet chamfering on pressure drop and heat transfer characteristics in confined air jet impingement choosing nozzle length to diameter ratio of 1.0. They concluded that chamfering the nozzle inlets reduce pressure drops without affecting much the heat transfer characteristics. Lee and Lee [22] studied the effect of nozzle aspect ratio on the local heat transfer characteristics of elliptic impinging jets on a heated flat plate experimentally. The stagnation Nusselt number was correlated for the aspect ratios and the nozzle-to-plate spacings tested during their study as $Nu_o \alpha (AR)^{-0.082}(l/de)^{-0.077}$. Zhao et al. [23] studied numerically the heat transfer performance of square, elliptic, and rectangular jets. They used the RNG k–ε turbulent model to conduct the impinging jet simulations. It was concluded that z/de of 5 to 6 give the best heat transfer for a circular jet while lower z/de show better performance for the square, rect-

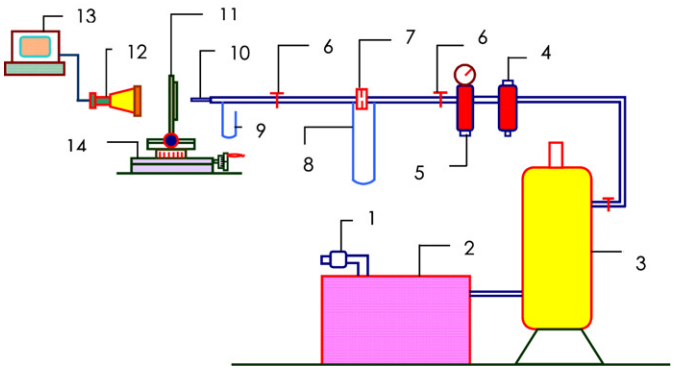

Fig. 1. Layout of experimental set-up. (1) Air filter. (2) Air compressor. (3) Air receiver. (4) Air filter. (5) Pressure regulator. (6) Needle valves. (7) Orifice plate. (8) Differential manometer. (9) Simple manometer. (10) Nozzle. (11) Impingement plate assembly. (12) Infra red camera. (13) Computer. (14) Traverse system.

Table 1
Detailed specifications of the nozzles

Type of nozzle	Breadth (mm)	Height (mm)	Equivalent diameter (*de*) (mm)	Hydraulic diameter (*d*) (mm)
Circular	20	20	20	20
Square	17	17	19.2	17
Rectangular	26.8	12	20.2	16.6

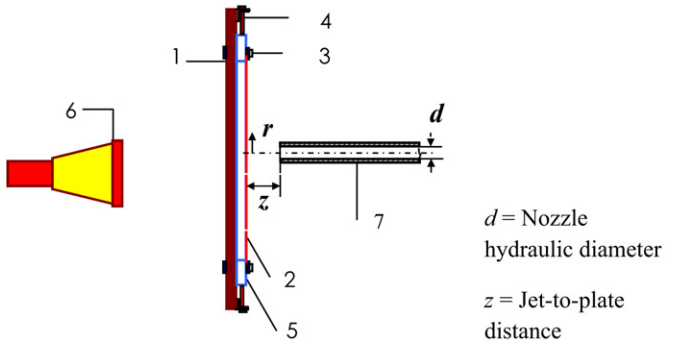

Fig. 2. Target plate assembly for heat transfer distribution. (1) Frame. (2) Stainless steel foil. (3) Clamping screw. (4) Stretching screw. (5) Copper bus bar. (6) I.R.Camera. (7) Nozzle.

angular, and elliptic jets. The exit conditions considered in this study are uniform flow with a fixed turbulence intensity of 2%. Neither the flow would be uniform nor the turbulence intensity be constant for a given nozzle shape in a practical situation. Hence, there is a need to study the effect of shape of the nozzle on the local heat transfer distribution in an impinging jet on a flat plate. More recently, Zhou and Lee [24] studied heat transfer and fluid flow characteristics due to impinging air jets from sharp-edged rectangular nozzle of aspect ratio of 4.0. The local heat transfer distributions along the minor axis and average Nusselt numbers are correlated with turbulence intensity.

The objective of the present paper is to study the influence of the shape of the nozzle (circular, square and rectangular) on

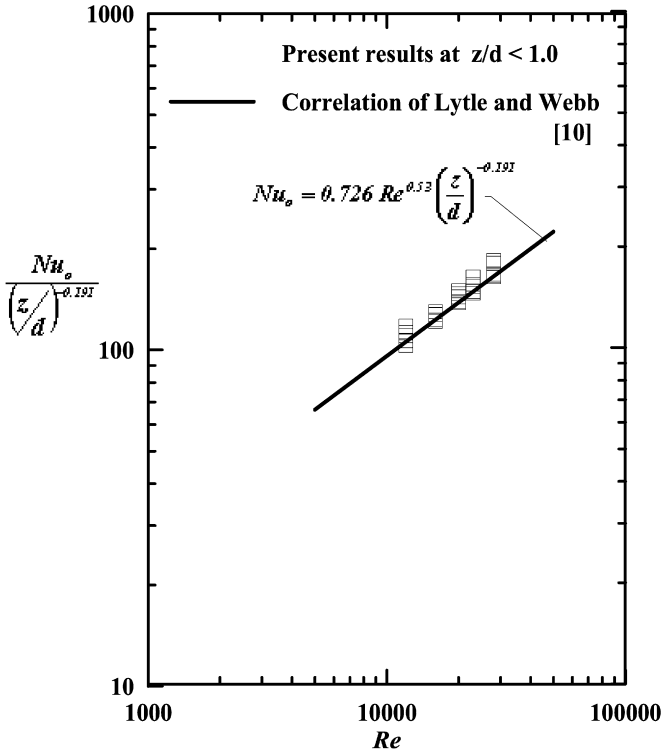

Fig. 3. Comparison of stagnation point Nusselt numbers with the correlation of Lytle and Webb [10].

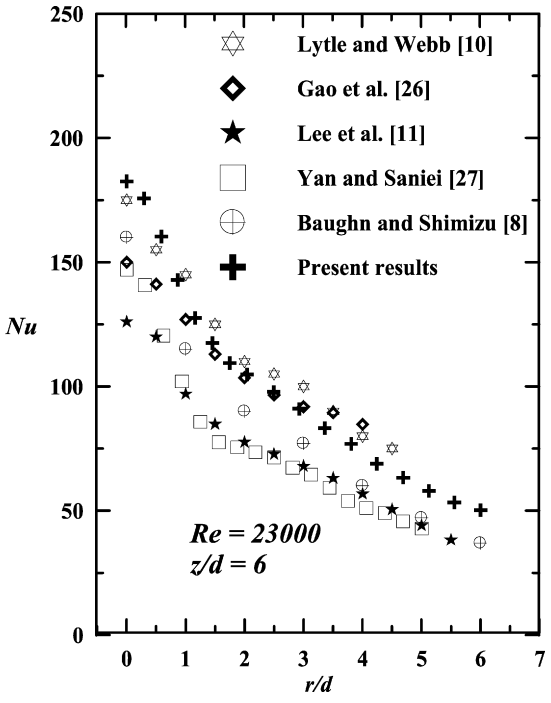

Fig. 4. Comparison of results with previous researchers for Nusselt number distribution.

the local heat transfer distribution to normally impinging submerged air jet on smooth and flat surface. The effect of jet to plate spacing (0.5 to 12 nozzle diameters) and Reynolds number (5000–15000) are studied for all the nozzles investigated.

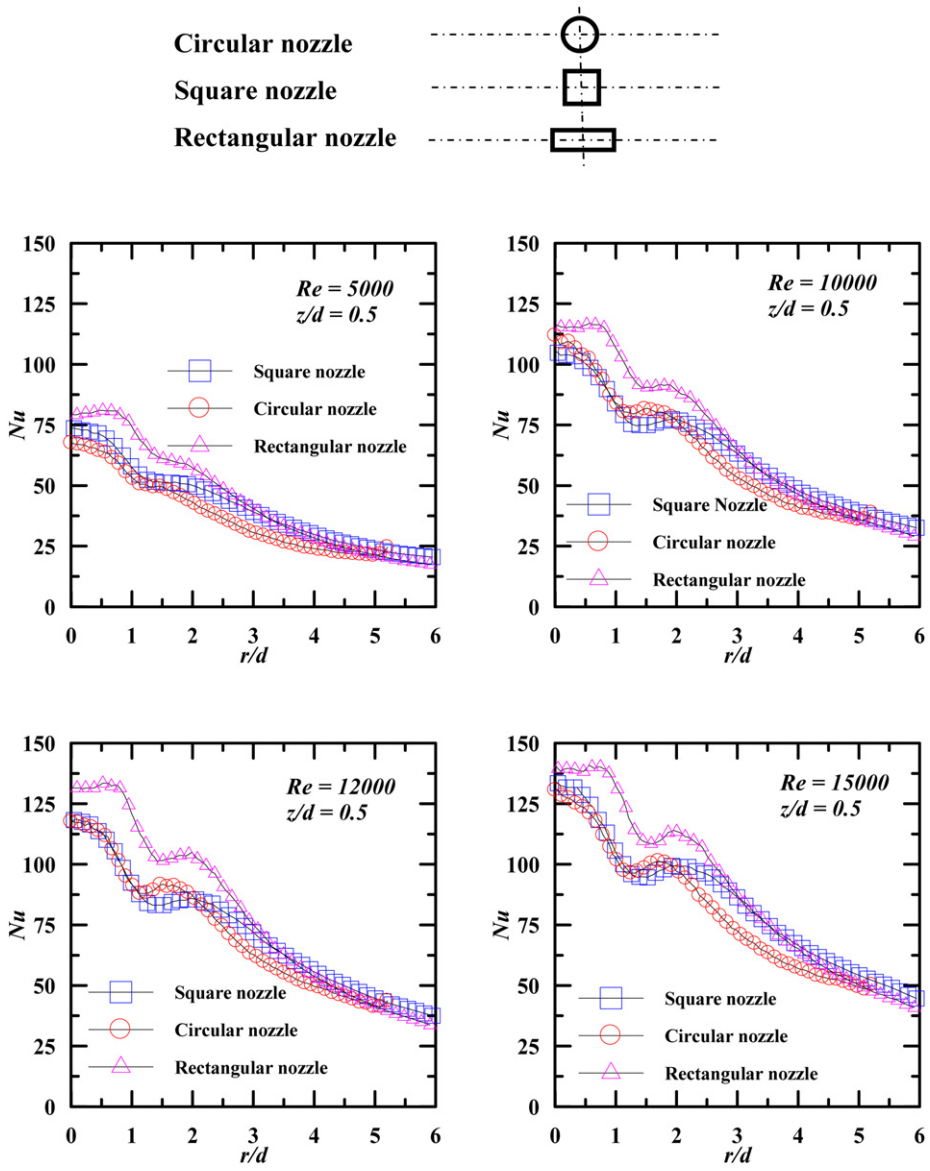

Fig. 5. Influence of shape of the nozzle on the local Nusselt number distribution along horizontal axis for different Reynolds numbers at a z/d of 0.5.

2. Experimental set up

The schematic lay-out of the experimental set-up is shown in Fig. 1. Air is supplied by an air compressor through a calibrated orifice flow meter. Air filter and pressure regulator are installed upstream of the orifice flow meter to filter the air and maintain the downstream pressure at 4 bar. The flow rate is controlled by two needle valves, one on each side of the orifice flow meter. The function of the upstream needle valve is not to allow cooling air to flow until the compressor has built up the pressure in its reservoir above 4 bar. Actual flow rate is controlled by the downstream needle valve. Three different nozzles, namely circular, square and rectangular of approximately equal exit area, are chosen. The length-to-equivalent diameter ratio (l/de) of nozzles is 50. The specifications of the different types of nozzles tested are listed in Table 1. The heater which also acts as an impinging plate (280 mm × 140 mm; 0.05 mm thick stainless steel foil) is clamped tightly and stretched between two copper bus bars. Approximately 15 mm of the foil on either side is sandwiched in the bus bars to ensure firm grip. The target plate assembly is as shown in Fig. 2. Because of the thinness of the foil, lateral conduction is negligible and surface provides constant heat flux situation, as reported by Lytle and Webb [10]. Thermal images are obtained from *IR* camera positioned on the side of the heater opposite the impinging nozzle.

One-dimensional energy balance across the heated plate shows that the temperature difference across it is negligibly small. Hence, the local temperature measured on the back surface is considered to be same as that on the impingement plane. The back surface of heater element is painted black using a thin coat of 'Matte finish Asian' paint which provides high emissivity (0.99) surface. During present experimentation, 'Thermoteknix' Ti200 infrared camera is used to collect the local temperature distribution over the target plate and obtained a resolution of about 0.65 mm per pixel. Power is supplied from *DC*

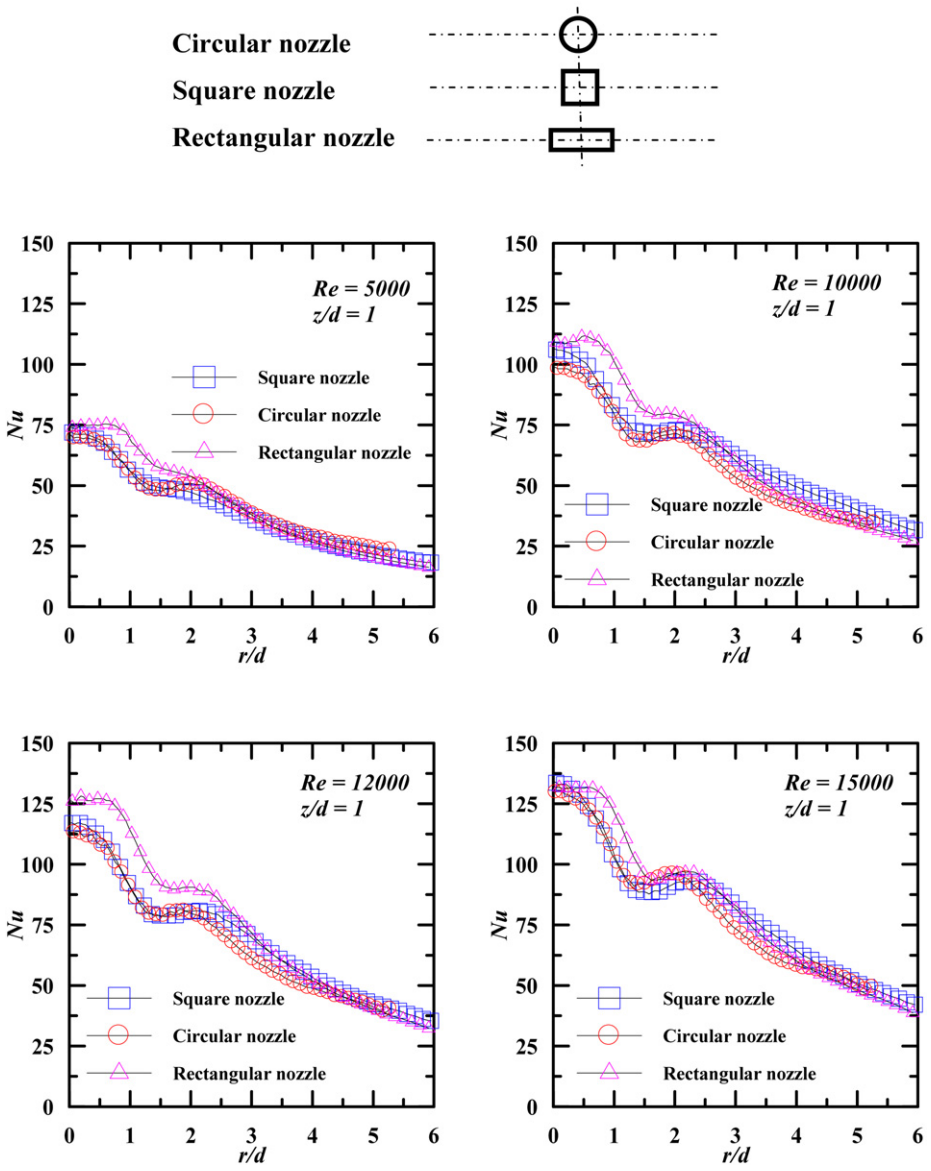

Fig. 6. Influence of shape of the nozzle on the local Nusselt number distribution along horizontal axis for different Reynolds numbers at a z/d of 1.

power source. Voltage taps are soldered at a distance of 206 mm apart on the target plate and wired to a multimeter to measure voltage. The current through the heater plate is directly read from the panel of DC power source. A Chromel–Alumel thermocouple (K-type) positioned just at the inlet of the nozzle is used to measure jet air temperature. The output of the thermocouple is measured by a millivoltmeter. A traverse system is used to set different jet-to-plate distances.

Thermal infrared camera reads the temperature of the plate depending on the emissivity value of the surface of the plate. Therefore, it is necessary to calibrate the emissivity of the surface. This is done by constructing a 100 mm size cubical tank from the same material as that of the target plate (i.e., stainless steel). This tank is painted with 'Matte Finish Asian' black paint to achieve uniform emissivity all over the surface. The tank is insulated from the five sides and one side is opened to the atmosphere. Tank is filled with water and is heated with a 500 W heater. A small motor driven stirrer is immersed in the water to maintain uniform temperature of the water bath. Two calibrated thermocouples are mounted on the exposed surface of the tank at two different locations. Initially, water in the tank is heated to the temperature of about 70 °C. Then, the heater is switched off and the temperature of the surface is allowed to decrease. The time constant of the temperature drop is about 3 minutes per 0.24 °C. This time is sufficient to obtain thermal images of the surface from the infrared camera and to note the thermocouple readings. The emissivity input to the images is then adjusted till the temperature read by the image is the same as that read by the thermocouples. This procedure is repeated for different temperatures of the exposed surface till it reached 35 °C. The average emissivity is found to be 0.99. The uncertainty in the temperature measurement is not more than ±0.5 °C.

Power loss from the exposed surface of the target plate due to natural convection and radiation is estimated experimentally.

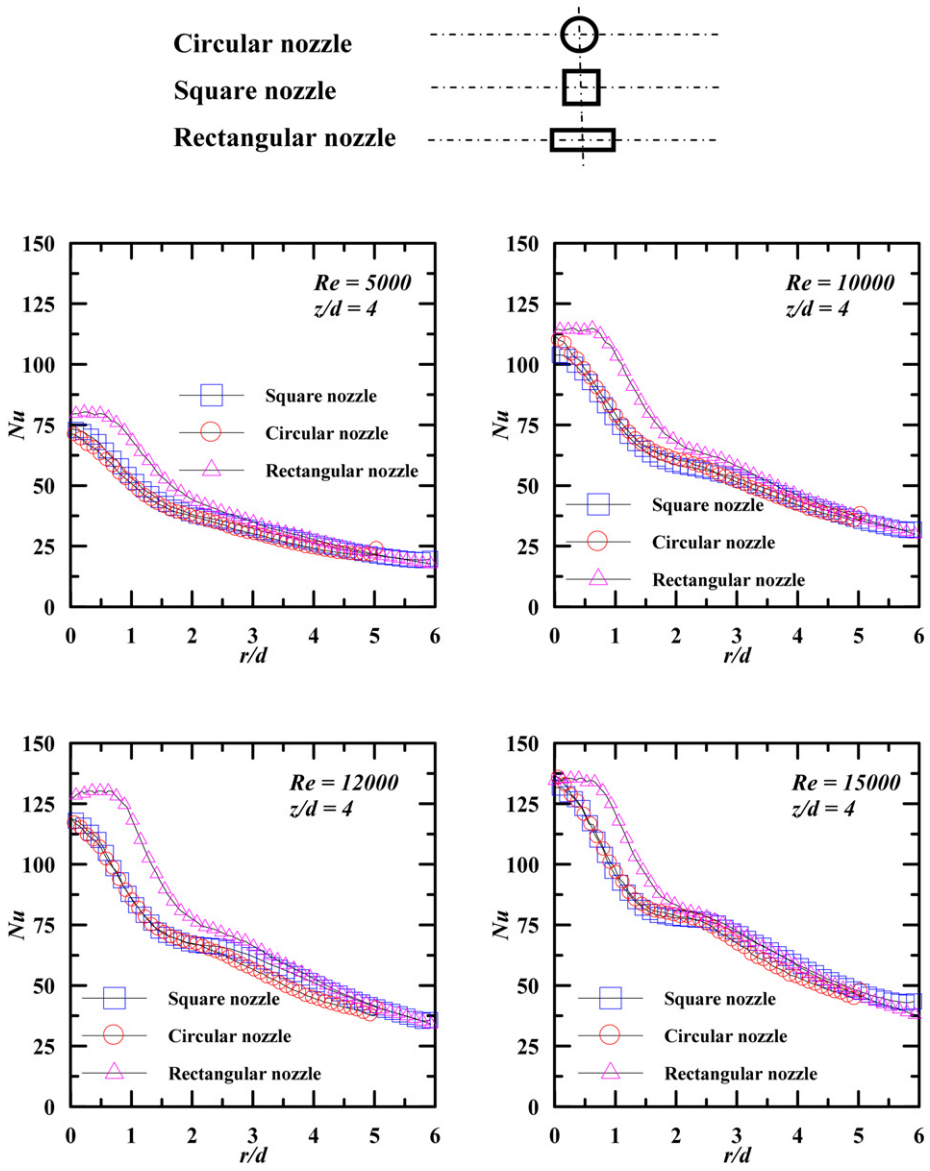

Fig. 7. Influence of shape of the nozzle on the local Nusselt number distribution along horizontal axis for different Reynolds numbers at a z/d of 4.

The corrections are included in calculation of local heat transfer coefficient.

3. Data reduction

The temperature distribution on the target plate is obtained from thermal images for each configuration. The Nusselt number for the smooth surface is calculated by

$$Nu = \frac{hd}{k} \tag{1}$$

$$h = \frac{q_{\text{conv}}}{T_r - T_j} \tag{2}$$

Heat transfer rate between impinging jet and target plate, q_{conv}, is estimated as follows:

$$q_{\text{conv}} = q_{\text{joule}} - q_{\text{loss}} \tag{3}$$

$$q_{\text{loss}} = q_{\text{rad}(f)} + q_{\text{rad}(b)} + q_{\text{nat}} \tag{4}$$

$$q_{\text{joule}} = \frac{VI}{A} \tag{5}$$

$$q_{\text{loss}} = q_{\text{rad}(f)} + q_{\text{rad}(b)} + q_{\text{nat.}} = \text{Estimated experimentally} \tag{6}$$

Uncertainties in the measurement of heat transfer coefficients are carried out using the method suggested by Moffat [25] and are around 3.4–7%.

4. Results and discussions

An experiment is carried out first with the long pipe nozzle which is closely similar to those of Lytle and Webb [10]. Fig. 3 shows that stagnation point Nusselt numbers of the present study are in good agreement (within 4.8%) with the correlations for low z/d (less than 1.0) of Lytle and Webb [10]. The local Nusselt number at a Reynolds number of 23 000 and z/d of 6 is compared with those of the earlier published data as shown in Fig. 4. It compares well with the results of Lytle and Webb [10] and Gao et al. [26] which use thin metal

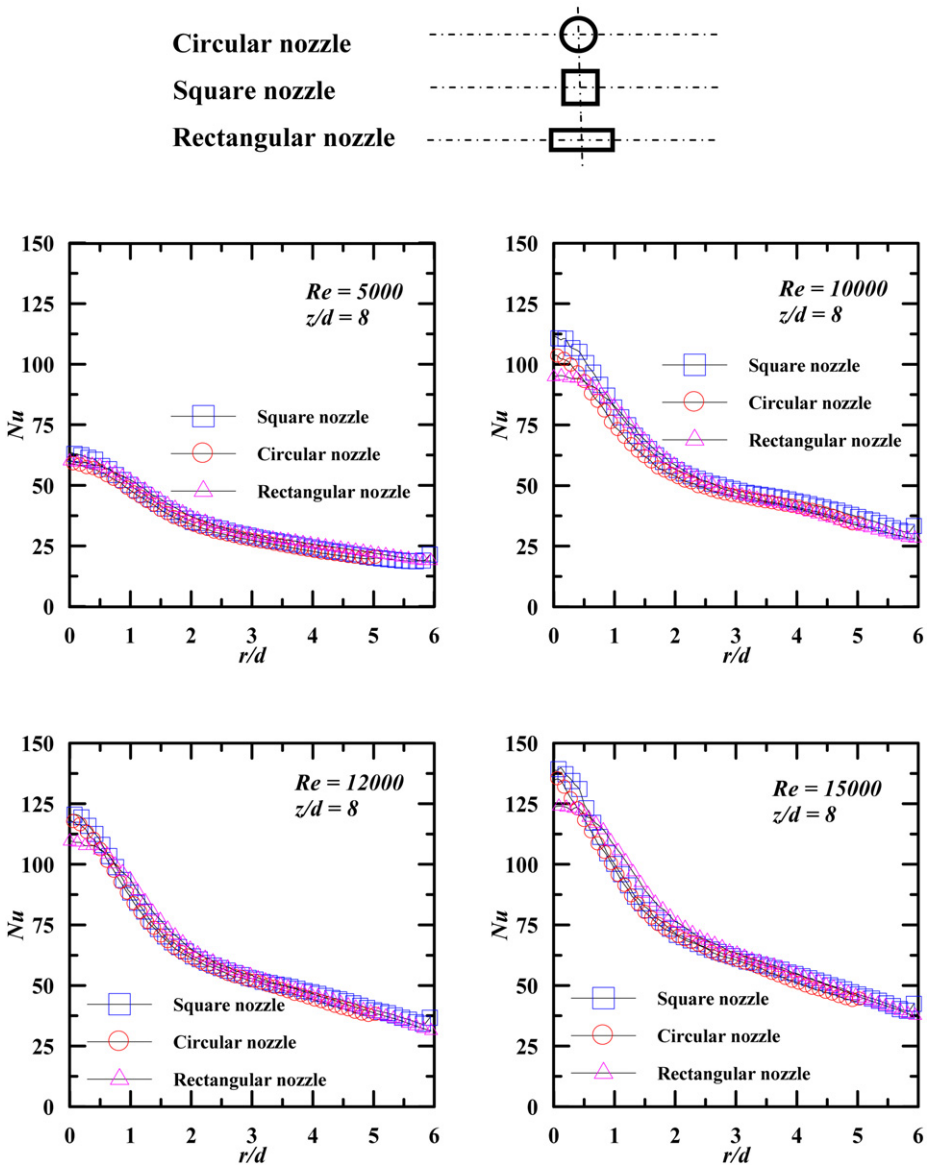

Fig. 8. Influence of shape of the nozzle on the local Nusselt number distribution along horizontal axis for different Reynolds numbers at a z/d of 8.

foil technique. It also compares well with the heat transfer results of Baughn and Shimizu [8], but is higher in the region away from the stagnation point. The heat transfer data of Lee et al. [11] and Yan and Saniei [27] are lower than the results of the present work. These differences may be attributed to the differences in the measurement techniques and thickness of the target plate.

The effect of shape of the nozzle on the local Nusselt number distribution at Reynolds number of 5000, 10000, 12000, and 15000 for nozzle-to-plate spacing (z/d) of 0.5 to 12.0 are studied experimentally. Figs. 5–9 show the local distribution of Nusselt numbers along the horizontal line through the stagnation point for nozzles of three different cross sections, viz. circular, square and rectangular. One pair of parallel sides of the cross section of square nozzle and longer parallel sides of nozzle of rectangular cross section are parallel to the horizontal. However, it is observed that there is distinct difference between the distribution of Nusselt numbers along the major and minor axis, for the rectangular jets.

Local Nusselt number distributions at $z/d = 0.5$ are shown in Fig. 5. It is observed that with increase in the Reynolds numbers, Nusselt number increases at all radial locations for all the three nozzle configurations. This may be due to increase of the momentum of jet with Reynolds number. The stagnation Nusselt numbers for square and circular nozzles are almost same at all Reynolds numbers. However, the Nusselt numbers at the stagnation point are higher for the rectangular jet by about 10% as compared to square and circular jets. This may be because of higher turbulent intensities at the nozzle exit and are carried to the stagnation region for rectangular nozzles. In the stagnation region i.e., up to r/d of 1.0, the Nusselt numbers decrease monotonically for circular and square nozzles. But, the Nusselt number values for rectangular nozzle in this region remain constant up to an $r/d = 0.75$ and then drop sharply till $r/d = 1.5$.

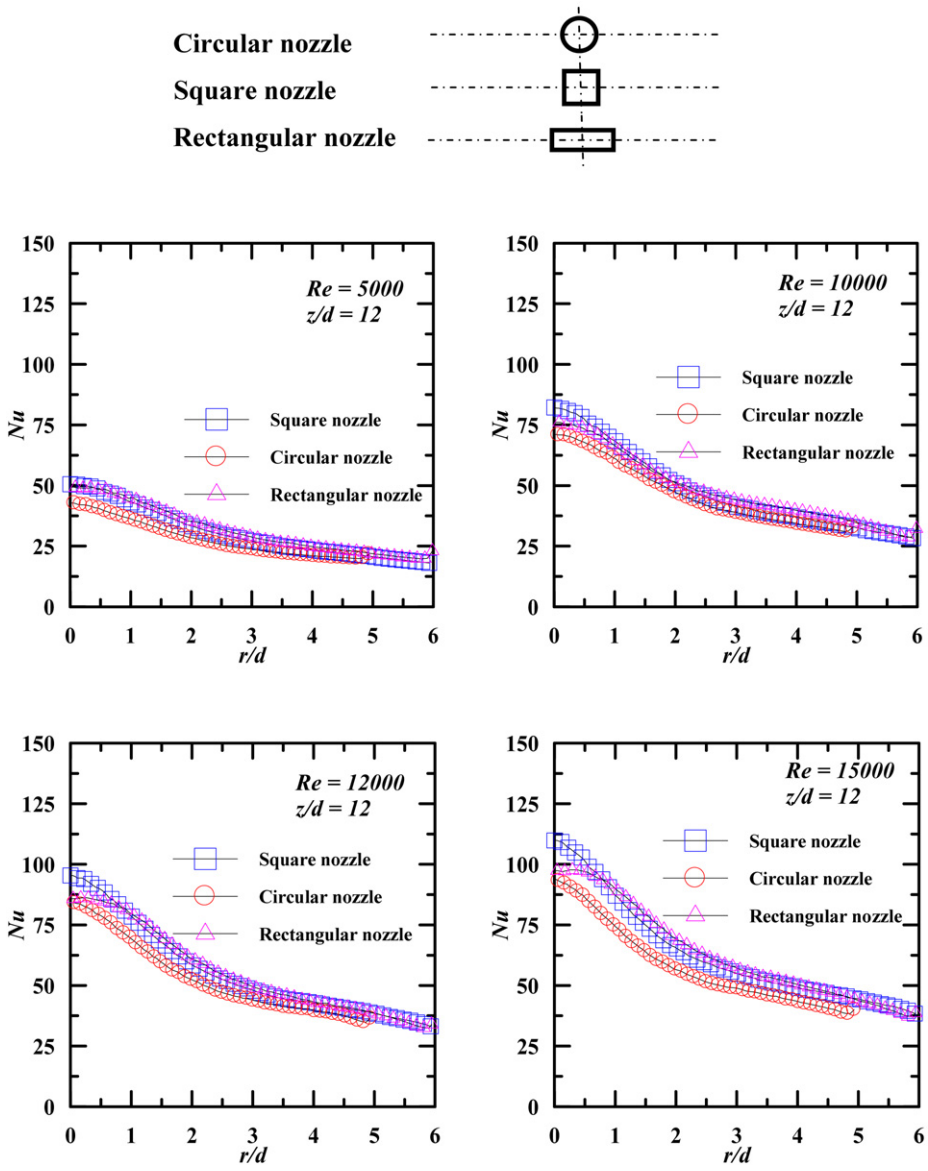

Fig. 9. Influence of shape of the nozzle on the local Nusselt number distribution along horizontal axis for different Reynolds numbers at a z/d of 12.

This may mark the end of stagnation region for impingement due to rectangular nozzle. For circular and square nozzles, a change in slope of the Nusselt number distribution is clearly observed at an $r/d = 1.2$ for all Reynolds numbers. But, a secondary peak is observed for Reynolds number of 12 000 and 15 000. The secondary peak is distinctly seen to occur at an r/d of about 1.75 for circular nozzle and at an r/d of about 2.0 for both square and rectangular nozzle. But, the secondary peaks diminish for lower Reynolds numbers. The trends in the Nusselt number distribution with rectangular nozzle show higher values at radial locations upto an r/d of about 2.4. Further, in the downstream the Nusselt numbers attenuate monotonically for all the three types of nozzles in an identical fashion.

Fig. 6 shows the distribution of local Nusselt numbers for all the three nozzles at $z/d = 1$. The trends are similar to the one observed at $z/d = 0.5$, but the stagnation values for rectangular nozzle case do not vary as much as at $z/d = 0.5$. However, the locations of secondary peaks shift away from the stagnation point. That is, for circular nozzle, secondary peak is observed at $r/d = 1.9$ and for square and rectangular nozzles it occurs at $r/d = 2.2$.

Fig. 7 shows the distribution of local Nusselt numbers for various Reynolds number at $z/d = 4$. However, the stagnation point Nusselt number values are almost same for all the three nozzles for a particular Reynolds number. The secondary peak is not distinctly observed. The distributions of the local Nusselt number for the square and circular nozzle are almost same and are marked by the beginning of the transition region at $r/d = 1.5$ which further extends up to an $r/d = 2.3$. For rectangular nozzle, the Nusselt number values in the stagnation region remain almost constant upto $r/d = 0.6$ and thereafter decreases monotonically. In the stagnation region, the Nusselt number values are higher for the rectangular jet as compared to the square and the circular jet.

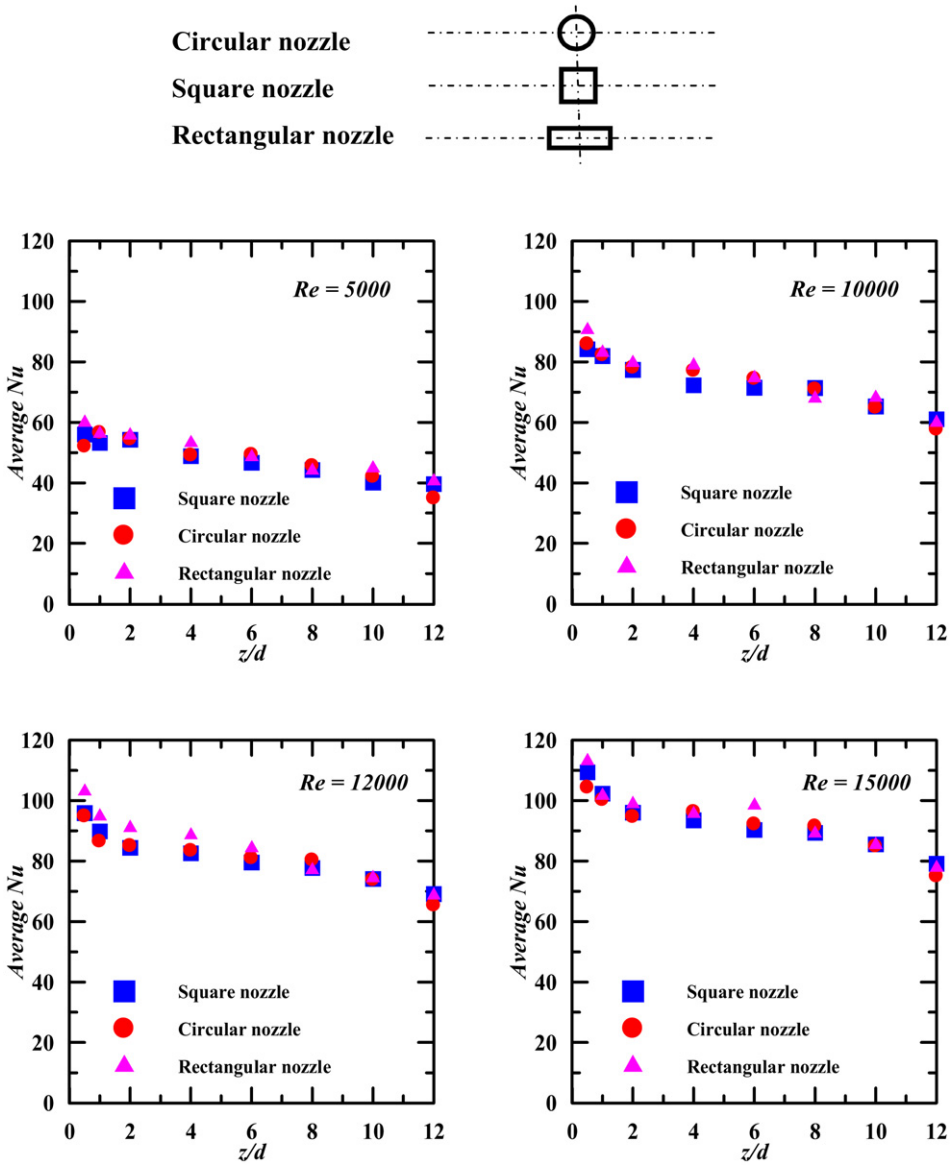

Fig. 10. Variation of average Nusselt number with nozzle-to-plate spacing at various Reynolds numbers for the square, circular and rectangular jets.

Local Nusselt number distributions for all the three nozzles at $z/d = 8$ and 12 are presented in Figs. 8 and 9, respectively. For Reynolds number of 5000 the effect of the nozzle shape is not distinctly observed. But, at higher Reynolds numbers the Nusselt number values for rectangular nozzle upto $r/d = 2.8$ are slightly higher than those for square and the circular nozzle. The effects of the Reynolds number for these z/d's are similar. At higher z/d's, it is observed that the results for all the three configurations collapse on a single curve.

The variation of average Nusselt number calculated over 3600 mm^2 area (60 mm × 60 mm) around the stagnation point with nozzle-to-plate spacing ratios, for all the Reynolds number studied is shown in Fig. 10. The average Nusselt number for a Reynolds number and at a particular z/d have the same values for all the three configurations. It is observed that average Nusselt numbers increase with the increase in Reynolds number for all the nozzle configurations. The average Nusselt number decreases with the increase in z/d for all the Reynolds number. But, for z/d's lower than 2, it is seen that average Nusselt numbers increase with decrease in z/d.

Fig. 11 shows the influence of z/d on the stagnation point Nusselt number at different Reynolds numbers for the square, circular and rectangular jets. It is observed that stagnation point Nusselt numbers increase with z/d from $z/d = 1.0$ up to around $z/d = 6.0$ and then slightly drop. This trend may be due to increase in turbulent intensity at the stagnation point with increase in z/d. The experimental results of Cooper et al. [28] show the dependence of the stagnation Nusselt number for $z/d \geqslant 2.0$ with near wall axial turbulent intensities. At $z/d = 2.0$, near wall axial turbulent intensities are around 5%. However, at $z/d = 4.0$ and at $z/d = 6.0$, near wall axial turbulent intensities are around 12.8%. Higher near wall axial turbulence intensity has been attributed to the spreading of mixing layer that originates from the rim of the nozzle to the jet axis.

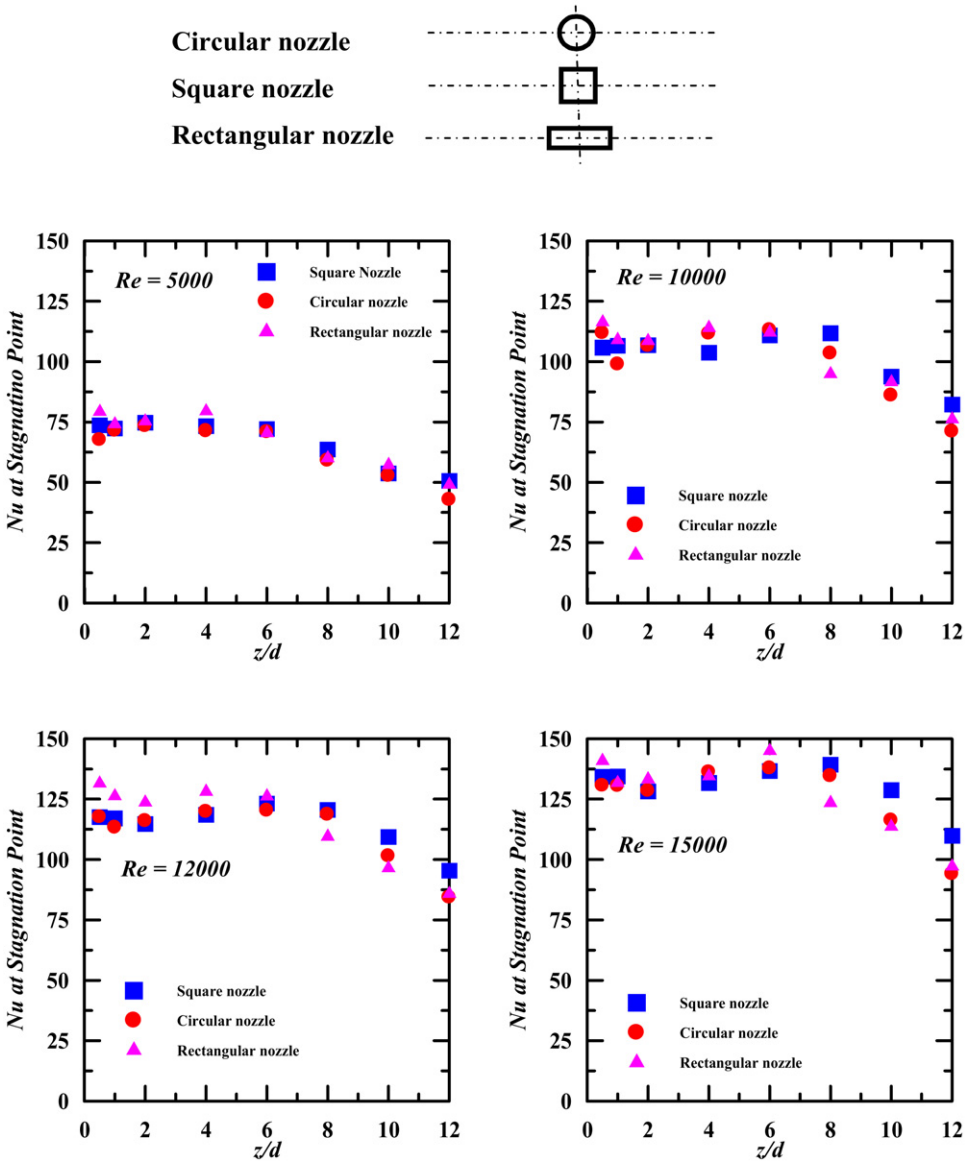

Fig. 11. Influence of z/d on the stagnation point Nusselt number at different Reynolds numbers for the square, circular and rectangular jets.

But, for z/d's lower than 1.0, it is seen that stagnation point Nusselt numbers increase with decrease in z/d. This increase in heat transfer at lower jet-to-plate spacing (<1.0) may be due to the acceleration of the fluid through the gap between target plate and nozzle exit.

The variations of local Nusselt numbers distribution along horizontal line on the impinged surface for all z/d's studied at Reynolds number of 5000 and 15 000 are shown in Fig. 15. For all the nozzles, it is observed that the location of the secondary peak shifts towards the stagnation point with decrease in the jet-to-plate distance. The increase in the value of Nusselt number at the secondary peak is observed to be higher with decrease in z/d. Increase in the Nusselt numbers at the secondary peak is more for $z/d = 0.5$. These observations are similar to the one reported by Lytle and Webb [10]. For $z/d = 4$ the secondary peak is not seen but sharp decrease in the slope of distribution of local Nusselt number distribution is observed. Further in the wall jet region, Nusselt numbers decay monotonically for all the three nozzles studied. For all the Reynolds numbers, it is seen that the Nusselt numbers decreases monotonically in the radial direction away from the stagnation point for z/d of 6 and higher. Instead of secondary peak, a mild decrease in the slope of distribution of local Nusselt numbers is observed.

Figs. 13, 14, and 15 show the Nusselt number distribution contours on the impingement surface, for different spacing ratios at Reynolds number of 15 000, for circular, square, and rectangular jets respectively. It is observed that at lower z/d's the contours retain the shape of the nozzle from which flow emerges, while at higher z/d's the contours tend to be axisymmetric. The similar trend was reported by Zhao et al. [23] for the velocity and the pressure contours. Zhao et al. [23] observed that the velocity and the pressure contours retain the shape of the orifice from which the flow emerges, which

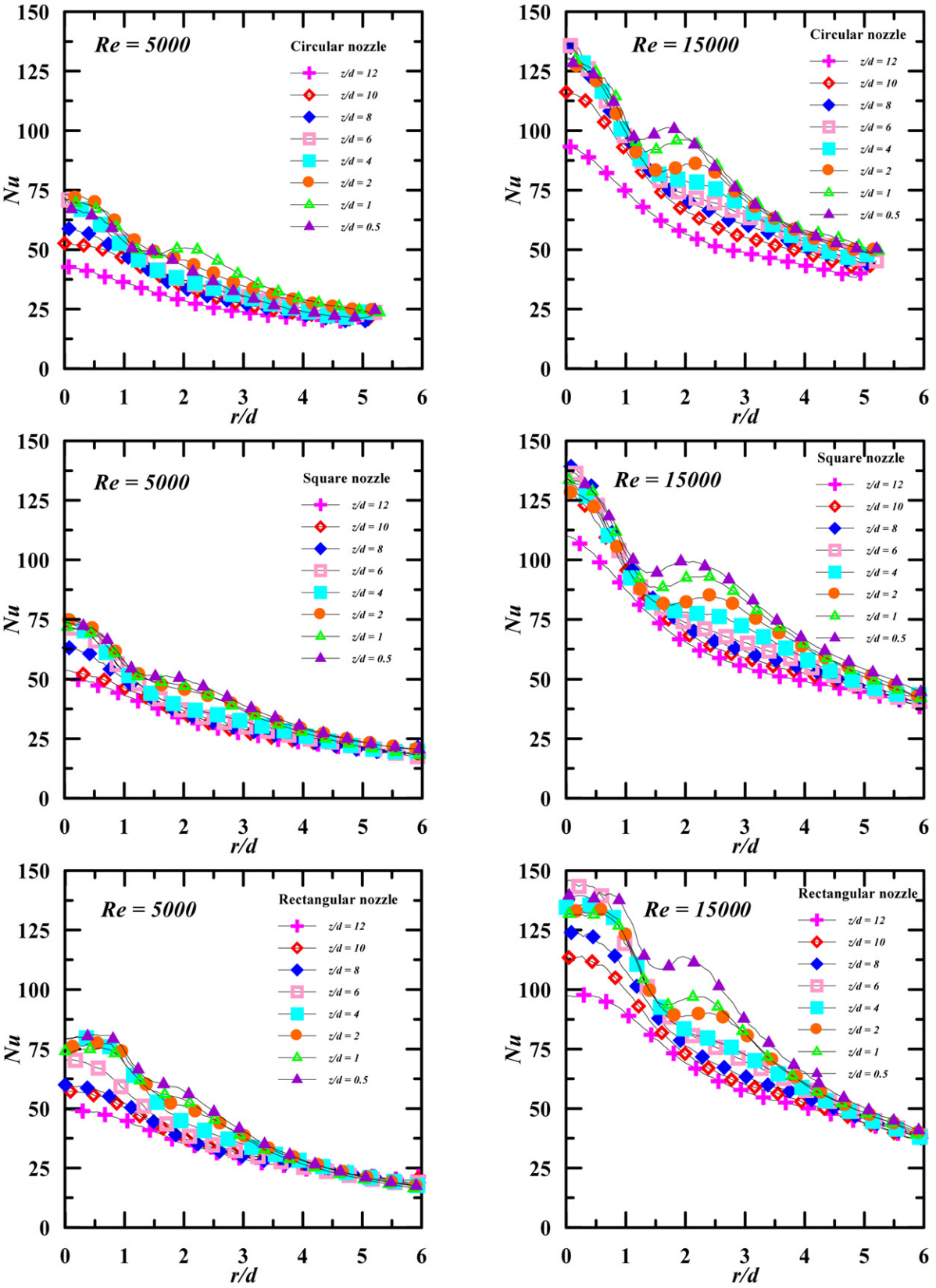

Fig. 12. Influence of z/d on the local Nusselt number distribution at Reynolds numbers of 5000 and 15 000 for the different nozzle shapes.

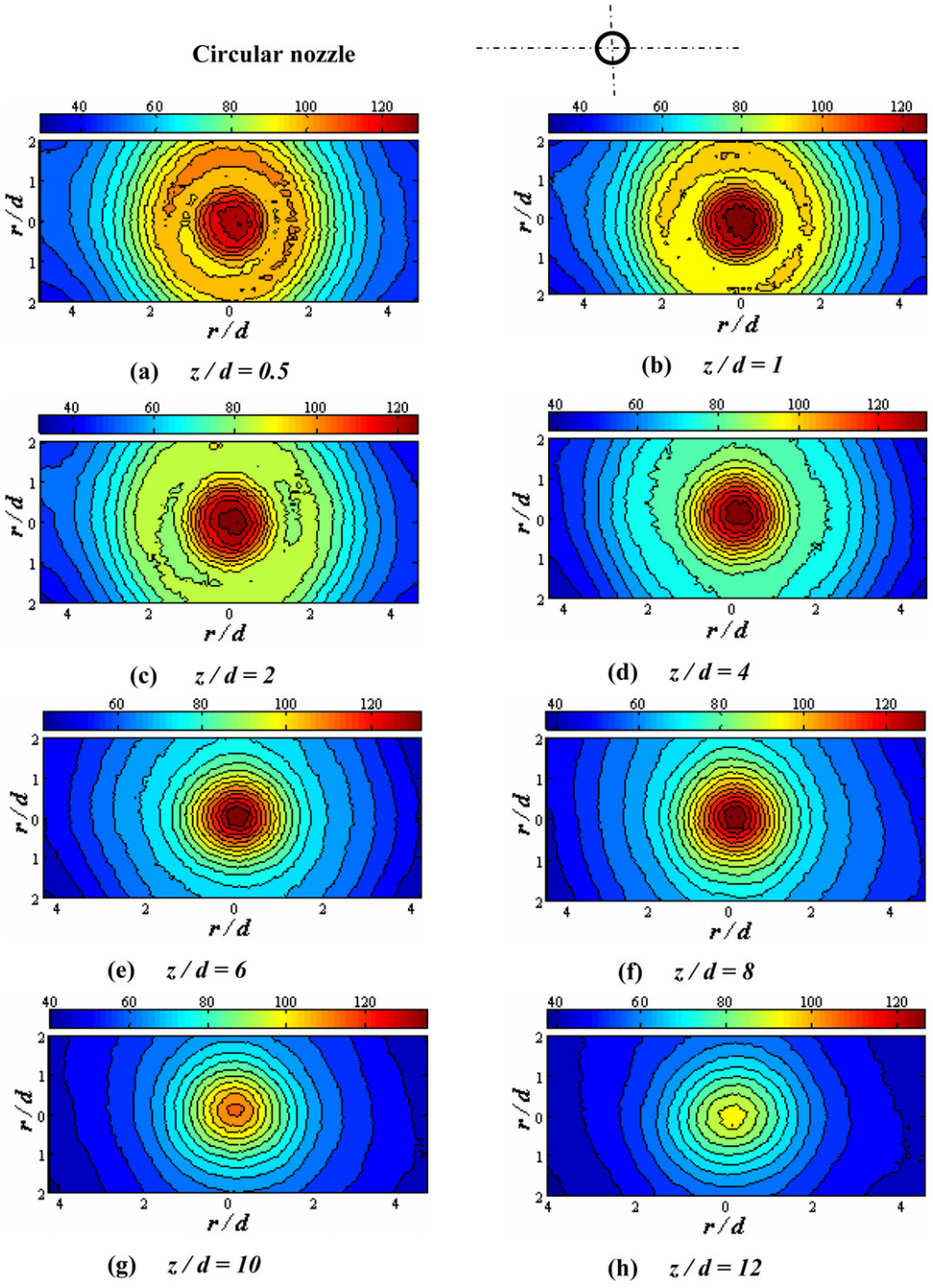

Fig. 13. Nusselt number distribution contours on the impingement surface for circular jet at different spacing ratios ($Re = 15\,000$).

further downstream the contours show a clear trend to increasingly axisymmetric. Locally high Nusselt number regions have been observed in the transition region at lower z/d's. This also explains the existence of secondary peaks at lower z/d's.

The pressure loss coefficient (K) for the different jet studied in this work is shown in Fig. 16 for various z/d's at different Reynolds number. It is observed that K for the circular jet is lowest and for the rectangular jet, it is highest, i.e., the maximum pumping power is required for the rectangular jet and least pumping power is required for the circular jet. The pressure loss coefficients for the circular nozzle are around 25% and 65% lower than those for the square nozzle, and rectangular nozzle respectively. It is observed that the pressure loss coefficient values are almost insensitive to z/d for all the three nozzles studied.

5. Comparison of the present results with those of Zhao et al. [23]

Table 2 shows the comparison of Nusselt number at the stagnation point for square and rectangular jet at different z/d ratios for a Reynolds number of 15000 with those of Zhao et al. [23]. It is observed that the stagnation point Nusselt numbers re-

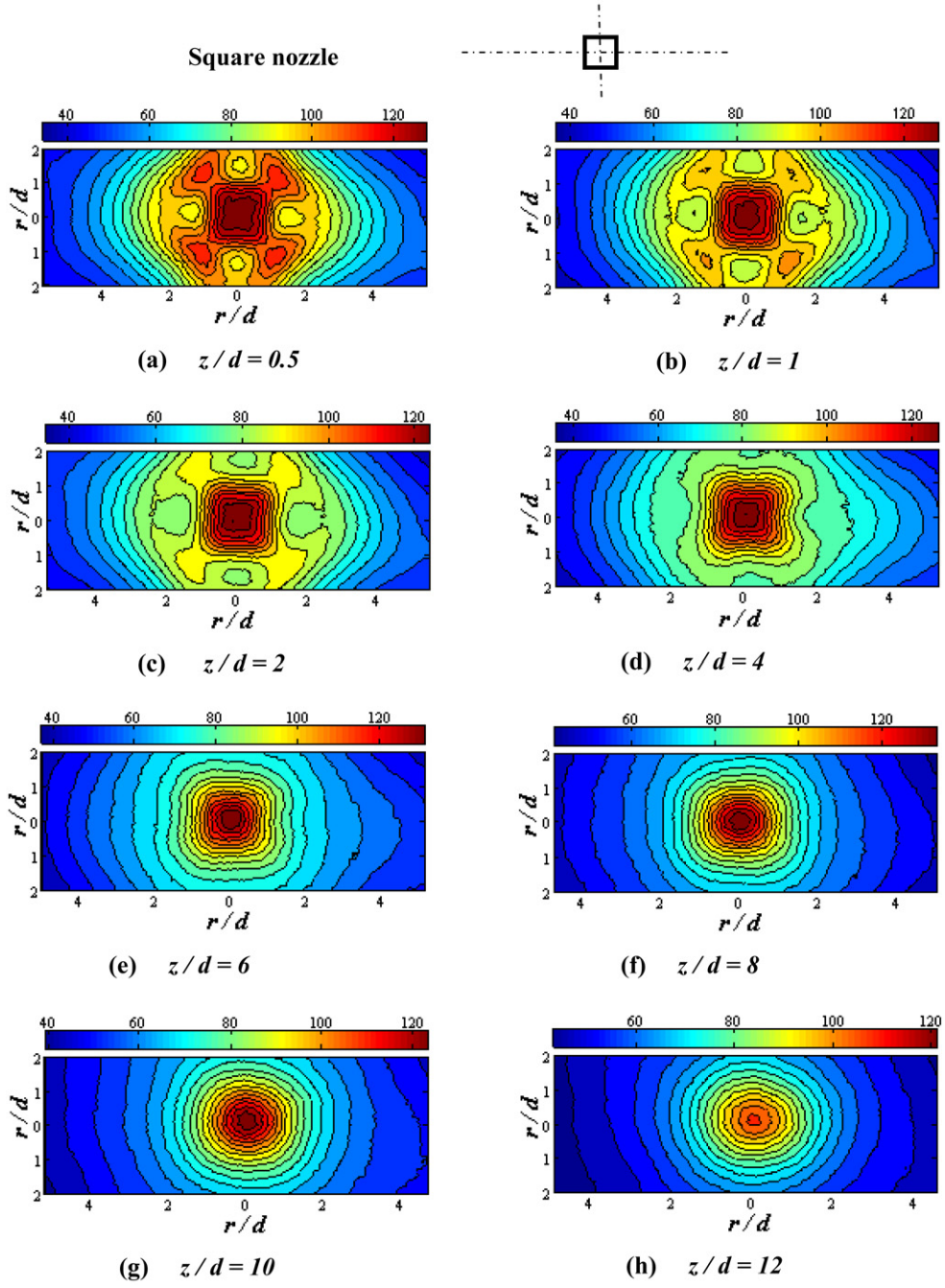

Fig. 14. Nusselt number distribution contours on the impingement surface for square jet at different spacing ratios ($Re = 15\,000$).

ported by Zhao et al. [23] are approximately 40% lower than those of the present results for both square and rectangular jets. This difference is due to the differences in the flow distribution at the exit of the nozzle and also the effect of confinement in numerical studies conducted by Zhao et al. [23].

Zhao et al. [23] considers uniform flow distribution and a constant turbulence intensity of 2% at the exit of all the nozzles (circular, square, rectangular and elliptical) studied by them. In the present study, the flow distribution is fully developed because the length to diameter ratio provided for all the nozzles is around $50d_e$. Also, the turbulence intensity for each nozzle shape may differ significantly.

Table 2
Comparison of stagnation point Nusselt numbers for different z/d

z/d	Square jet ($Re = 15\,000$)		Rectangular jet ($Re = 15\,000$)	
	Present experimental results	Zhao et al. [23] (Numerical results)	Present experimental results	Zhao et al. [23] (Numerical results)
2	128	72	133	78
4	132	78	135	84
6	137	84	145	78
8	139	63	124	64

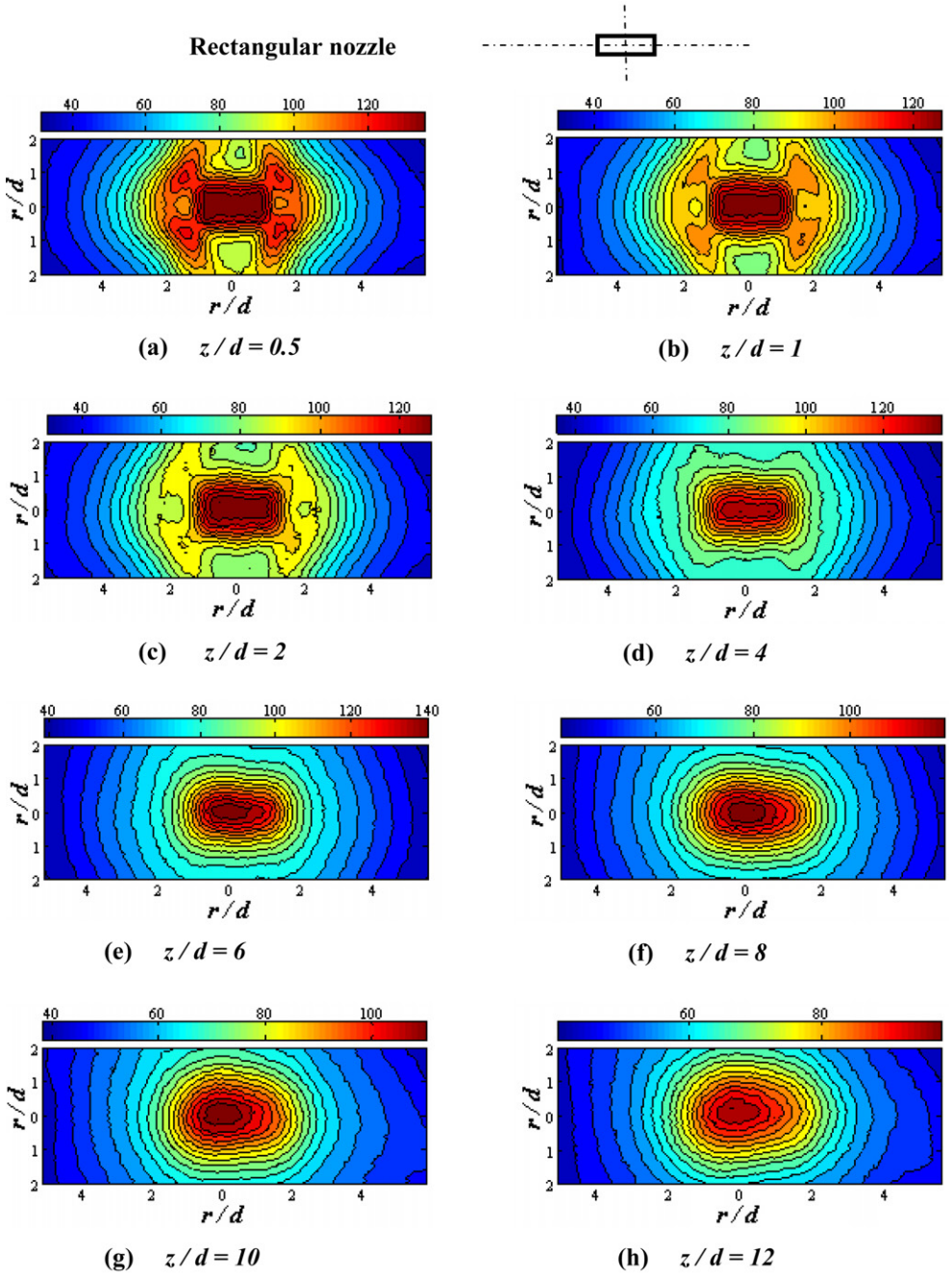

Fig. 15. Nusselt number distribution contours on the impingement surface for rectangular jet at different spacing ratios ($Re = 15\,000$).

6. Conclusions

The effects of the shape of the nozzle on impinging jet heat transfer is experimentally investigated at different Reynolds numbers and nozzle-to-plate spacing. Three different nozzles cross sections namely circular, square, and rectangular are covered in this study. The following are the main conclusions that may be drawn from this study

- The effect of Reynolds number on the performance of non-circular jets is similar to that for the circular jet; with increase of Reynolds number, the heat transfer rate increases. The heat transfer characteristics of square and circular jets show much similarity.
- There is a distinct difference between distribution of Nusselt numbers along the major and minor axis for rectangular jet.
- It is observed that, upto z/d of 6, the Nusselt number distribution along the horizontal axis for rectangular jet is higher in the stagnation region than those of circular and square jets.
- The average Nusselt number calculated over 3600 mm^2 area (60 mm × 60 mm), around the stagnation point is almost same for all the nozzle configurations tested.

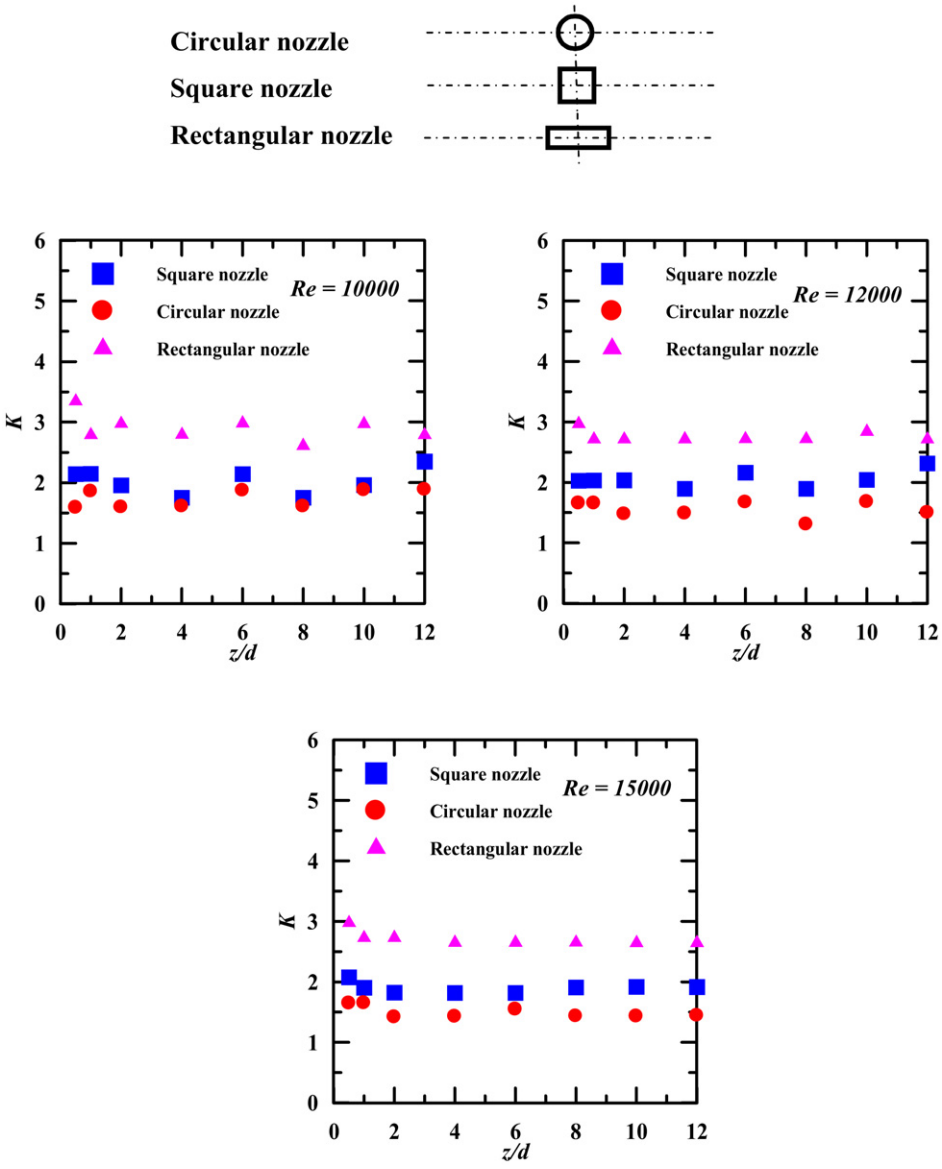

Fig. 16. Variation of K with nozzle-to-plate spacing at various Reynolds numbers for the square, circular and rectangular jets.

- Pressure loss coefficient is lowest for the circular jet and highest for rectangular jet.

References

[1] J.N.B. Livingood, P. Hrycak, Impingement heat transfer from turbulent air jets to flat plates — A literature survey, NASA Technical Memorandum (NASA TM X-2778), 1970.

[2] H. Martin, Heat and mass transfer between impinging gas jets and solid surfaces, Advances in Heat Transfer 13 (1977) 1–60.

[3] K. Jambunathan, E. Lai, M.A. Moss, B.L. Button, A review of heat transfer data for single circular jet impingement, International Journal of Heat and Fluid Flow 13 (1992) 106–115.

[4] R. Viskanta, Heat transfer to impinging isothermal gas and flame jets, Experimental Thermal and Fluid Science 6 (1993) 111–134.

[5] R. Gardon, J. Cobonpue, Heat transfer between a flat plate and jets of air impinging on it, in: Int. Developments in Heat Transfer, ASME, 1962, pp. 454–460.

[6] R. Gardon, C. Akfirat, The role of turbulence in determining the heat transfer characteristics of impinging jets, International Journal of Heat and Mass Transfer 8 (1965) 1261–1272.

[7] R. Gardon, C. Akfirat, Heat transfer characteristics of impinging two dimensional air jets, Journal of Heat Transfer 88 (1966) 101–108.

[8] J.W. Baughn, S. Shimizu, Heat transfer measurements from a surface with uniform heat flux and an impinging jet, Journal of Heat Transfer 111 (1989) 1096–1098.

[9] P. Hrycak, Heat transfer from round impinging jets to a flat plate, International Journal of Heat and Mass Transfer 26 (1983) 1857–1865.

[10] D. Lytle, B.W. Webb, Air jet impingement heat transfer at low nozzle plate spacings, International Journal of Heat and Mass Transfer 37 (1994) 1687–1697.

[11] D.H. Lee, J. Song, C.J. Myeong, The effect of nozzle diameter on impinging jet heat transfer and fluid flow, Journal of Heat Transfer 126 (2004) 554–557.

[12] A.H. Beitelmal, A.J. Shah, M.A. Saad, Analysis of an impinging two dimensional jet, Journal of Heat Transfer 128 (2006) 307–310.

[13] J.H. Lienhard, Heat transfer by impingement of circular free-surface liquid jets, in: 18th National and 7th ISHMT-ASME Heat and Mass Transfer Conference, January 4–6, 2006.

[14] H.M. Hofmann, M. Kind, H. Martin, Measurements on steady state heat transfer and flow structure and new correlations for heat and mass trans-

fer in submerged impinging jets, International Journal of Heat and Mass Transfer 50 (2007) 3957–3965.

[15] T.S. O'Donovan, D.B. Murray, Jet impingement heat transfer—Part I: Mean and root-mean-square heat transfer and velocity distributions, International Journal of Heat and Mass Transfer 50 (2007) 3291–3301.

[16] T.S. O'Donovan, D.B. Murray, Jet impingement heat transfer—Part II: A temporal investigation of heat transfer and local fluid velocities, International Journal of Heat and Mass Transfer 50 (2007) 3302–3314.

[17] Y. Pan, J. Stevens, B.W. Webb, Effect of nozzle configuration on transport in the stagnation zone of axisymmetric, impinging free surface liquid jets: Part 1—Turbulent flow structure, Journal of Heat Transfer 114 (1992) 874–879.

[18] J. Stevens, Y. Pan, B.W. Webb, Effect of nozzle configuration on transport in the stagnation zone of axisymmetric, impinging free surface liquid jets: Part 2—Local heat transfer, Journal of Heat Transfer 114 (1992) 880–886.

[19] S.V. Garimella, B. Nenaydykh, Nozzle-geometry effects in liquid jet impingement heat transfer, International Journal of Heat and Mass Transfer 39 (1996) 2915–2923.

[20] J. Lee, S.-J. Lee, The effect of nozzle configuration on stagnation region heat transfer enhancement of axisymmetric jet impingement, International Journal of Heat and Mass Transfer 43 (2000) 3497–3509.

[21] L.A. Brignoni, S.V. Garimella, Effects of nozzle inlet chamfering on pressure drop and heat transfer in confined air jet impingement, International Journal of Heat and Mass Transfer 43 (2000) 1133–1139.

[22] J. Lee, S.-J. Lee, The effect of nozzle aspect ratio on stagnation region heat transfer characteristics of elliptic impinging jet, International Journal of Heat and Mass Transfer 43 (2000) 555–575.

[23] W. Zhao, K. Kumar, A.S. Mujumdar, Flow and heat transfer characteristics of confined noncircular turbulent impinging jets, Drying Technology 22 (2004) 2027–2049.

[24] D.W. Zhou, S.-J. Lee, Forced convective heat transfer with impinging rectangular jets, International Journal of Heat and Mass Transfer 50 (2007) 1916–1926.

[25] R.J. Moffat, Describing the uncertainties in experimental results, Experimental Thermal and Fluid Science 1 (1988) 3–17.

[26] N. Gao, H. Sun, D. Ewing, Heat transfer to impinging round jets with triangular tabs, International Journal of Heat Mass Transfer 46 (2003) 2557–2569.

[27] X. Yan, N. Saniei, Heat transfer from an obliquely impinging circular air jet to a flat plate, International Journal of Heat and Fluid Flow 18 (1997) 591–599.

[28] D. Cooper, D.C. Jackson, B.E. Launder, G.X. Liao, Impingement jet studies for turbulence model assessment—I. Flow-field experiments, International Journal of Heat and Mass Transfer 36 (1993) 2675–2684.